



PAPER

Evaluating HARQ Protocols for Mobile and Interactive Applications in Underwater Acoustic Wireless Sensor Networks

Agnel Shyam Kumar C. ,
Christhu Raj M. R.  

SRM Institute of Science
and Technology,
Kattankulathur, India

christhm1@srmist.edu.in

ABSTRACT

Underwater acoustic wireless sensor networks (UWSNs) play a vital role in supporting mobile and interactive applications such as real-time oceanographic monitoring, remote infrastructure inspection, and mission-critical maritime operations. However, the unique characteristics of underwater acoustic communication—including limited bandwidth, long propagation delays, and high error rates—pose significant challenges to achieving reliable, low-latency, and energy-efficient data delivery for mobile users. This paper presents a comparative performance evaluation of three hybrid automatic repeat request (HARQ) protocols, namely Type-I HARQ, Chase Combining HARQ (CC-HARQ), and Incremental Redundancy HARQ (IR-HARQ), within a realistic UWSN environment simulated using the RIVERBED platform. The analysis focuses on key performance metrics relevant to mobile and interactive applications, including packet delivery ratio, end-to-end delay, and energy consumption. Simulation results demonstrate that IR-HARQ provides superior reliability and energy efficiency, particularly under low signal-to-noise ratio conditions, making it well suited for interactive mobile access to underwater sensing data. By employing a realistic acoustic channel model rather than idealised assumptions, this study offers practical insights into the design of robust and adaptive communication mechanisms for mobile-centric UWSN deployments. The findings support the development of efficient underwater communication frameworks that enhance the quality of experience for mobile and interactive applications.

KEYWORDS

underwater acoustic wireless sensor networks (UWSNs), energy efficiency, incremental redundancy hybrid automatic repeat request (IRHARQ), stochastic network calculus, moment-generating function (MGF), delay bound, riverbed modeler, multipath fading, doppler spread, QoS provisioning

Agnel Shyam Kumar, C., Christhu Raj, M. R. (2026). Evaluating HARQ Protocols for Mobile and Interactive Applications in Underwater Acoustic Wireless Sensor Networks. *International Journal of Interactive Mobile Technologies (iJIM)*, 20(9), pp. 108–123. <https://doi.org/10.3991/ijim.v20i09.61487>

Article submitted 2026-01-05. Revision uploaded 2026-03-21. Final acceptance 2026-03-30.

© 2026 by the authors of this article. Published under CC-BY.

1 INTRODUCTION

The underwater acoustic channel is characterised by a path loss that increases non-linearly with both the propagation range and signal frequency at a physical layer due to viscous relaxation absorption by dissolved molecular species. The speed of sound is not a fixed constant but a function of temperature, salinity, and hydrostatic pressure according to empirically derived profile functions (e.g., the Munk canonical profile), resulting in ray bending and propagation zones that have significant impact on link budgets. The channel of the seabed is further compromised by wideband ambient noise whose spectral density contains contributions from distant freight, wind-borne bubble levitation, biological entities, and thermally activated molecules. Compounding these effects, platform motion, either of the sensor node (SN) due to ocean currents or of an AUV relay, results in Doppler frequency shifts, and at the network layer, UA-WSNs are subject to additional constraints due to the limited and non-renewable energy that can be used by submerged nodes, battery replacement or recharging of a cable is operationally unfeasible in many deployment scenarios. It thus must mediate between the contradictory requirements of reliability achieved via error-control constructs like hybrid automatic repeat request (HARQ) and energy efficiency, measured as the total amount of successfully conveyed information bits with respect to all energy consumed. These two goals are not orthogonal to one another such that well-designed adaptive HARQ can provide energy-efficient operation through a larger per-transmission success probability by reducing the rolling mean number of transmissions required and thus improving reliability.

In particular, incremental redundancy hybrid automatic repeat request (IR-HARQ)—where each successive round of retransmission supplies fresh redundancy bits to allow for a decrease in code rate and soft-information combination at the destination—is well suited to this goal. Because each HARQ round continually reduces the effective code rate, for example, approaching Shannon capacity from above while the transmitter power is fixed, IR-HARQ provides a power-efficient design. The tricky part is to adjust IR-HARQ design such that it accounts for the distinctive characteristics of underwater acoustic channel nature, i.e., the considerably long round-trip propagation delay (upwards of tens or hundreds of milliseconds), coherence time associated with the fading process (which indicates if successions of HARQ rounds are dependent or independent), and energy cost associated with decoding activities at a battery-limited sensor node. Traditional performance analysis of communication protocols operating in real-time complex stochastic environments heavily depends on the mathematical machinery surrounding Markov chains as well as their extensions, providing state wise accuracy but at a significantly higher runtime cost, becoming unwieldy with an increasing number of HARQ rounds, queue lengths, and channel states.

Stochastic network calculus (SNC) offers a clean and scalable approach: by abstracting traffic and channel service into stochastic bounds obtained from the moment-generating function (MGF) of the random underlying processes, SNC achieves per-flow, probabilistic QoS guarantees on delay, throughput, and packet loss. Different from deterministic network calculus, which results in worst-case bounds that are usually quite conservative for wireless channels, SNC provides bounds with adjustable violation probabilities assigned according to the statistical QoS needs of the modern UA-WSN applications. Simulation validation of the proposed protocol is done using Riverbed Modeller (previously known as OPNET Modeller), which is a commercial event-driven hierarchical network simulator complete with

user-definable protocol process models implemented in Proto-C simulation language. Riverbed Modeller's layered architecture spanning application, transport, network, MAC, and PHY tiers is well-suited to UA-WSN protocol evaluation, as it faithfully captures the interaction between queuing dynamics, protocol state machines, and physical-channel impairments within a unified simulation environment.

1.1 Motivation and problem statement

The design of energy-efficient and reliable UA-WSN downlink protocols entails three interlocked sub-problems. First, a physically accurate and mathematically tractable channel model must be established that captures the dominant impairments of the underwater acoustic medium without sacrificing analytical tractability. Second, an IR-HARQ protocol must be designed that optimises the trade-off between retransmission overhead, energy consumption per delivered bit, and end-to-end delay bound. Third, a rigorous analytical framework must be developed that provides provably valid, probabilistic QoS guarantees for this protocol over the characterised channel, validated by high-fidelity simulation. The present paper addresses all three sub-problems in an integrated manner, with explicit emphasis on the interplay between energy efficiency, reliability, and delay.

1.2 Contributions

The principal contributions of this paper may be summarised as follows:

(C1) **Comprehensive UA-WSN Channel Model:** We develop a physically motivated channel model that integrates the Thorp frequency-dependent absorption formula, the Wenz empirical ambient noise model, Nakagami-m distributed multipath fading with parameters calibrated to measured shallow-water and deep-water UA-WSN environments, and a statistical Doppler spread model derived from first principles of platform kinematics and ray geometry. The model is cast in a form amenable to MGF-based SNC analysis.

(C2) **Energy-Efficient IR-HARQ Protocol:** We introduce an IR-HARQ protocol augmented with an energy-efficiency controller that adaptively manages transmit power, retransmission round count, and inter-round idle intervals to maximise energy efficiency (throughput per unit power) subject to a maximum end-to-end delay constraint. The protocol accounts for the residual energy budget of the SN and the statistical properties of the acoustic channel.

(C3) **SNC Analytical Framework:** We derive stochastic arrival and service curves for the proposed system using MGF-based bounding techniques. Closed-form or semi-closed-form expressions are obtained for: (i) the probabilistic delay bound violation probability; (ii) the average throughput lower bound; (iii) the average bit error rate (BER); and (iv) the packet loss probability. The SNC framework is more scalable than Markov chain analysis and yields tighter bounds than deterministic network calculus.

(C4) **Riverbed Modeller Simulation:** We implement the complete protocol stack—acoustic PHY, IR-HARQ finite state machine, energy-efficiency controller, MAC sublayer, and transport layer—as custom process models in Riverbed Modeller. Extensive Monte Carlo simulation over 10^6 slots with 10^3 independent channel realisations validates the analytical bounds and benchmarks the proposed scheme against four alternative protocols.

(C5) **Comprehensive Performance Benchmarking:** We provide a multi-dimensional performance comparison—encompassing BER, throughput, energy efficiency, delay, and packet loss—across a wide range of system parameters, sea states, and node velocities, offering system designers a detailed design space characterisation.

2 SIGNIFICANCE FOR REAL-WORLD UA-WSN DEPLOYMENTS

The practical significance of the proposed framework extends beyond its theoretical novelty. In real-world UA-WSN deployments such as the NEPTUNE Canada cabled observatory network, the ALOHA cabled observatory in the North Pacific, and the numerous temporary mooring networks deployed for oceanographic research campaigns, node energy management is a primary operational constraint. Battery replacement for nodes deployed at depths of 1000–4000 m requires remotely operated vehicle (ROV) intervention at a typical cost of USD 10,000–50,000 per dive, making energy efficiency economically as well as technically critical. The proposed IR-HARQ energy-efficiency controller reduces the per-packet energy consumption by 32.4% compared to the per-data packet energy consumption of $E[N_{\text{rounds}}] = 2.87$ (CC-HARQ baseline) down to $E[N_{\text{rounds}}] = 1.94$ (proposed scheme) at nominal SNR with its reduction in average number of retransmission rounds for the delivery of data packets. For instance, a deployment scenario deployed for 2 years which consists of 100 nodes each transmitting (10^6) packets leads to approximately 3.24×10^7 packet-transmissions' worth of energy saving, translating into extending battery lifetime from (15) months to over (22) months. This 47% extension in ROV lifetime is readily converted to decreased ROV maintenance costs and increased data collection availability, both of which are topmost goals of ocean observatory operators. Such variety of bound delay guarantees provided by the SNC frameworks are also practically important for time-sensitive UA-WSN applications. Real-time packet delivery within the prescribed latency window (generally less than 1–5 seconds for seismic alerts and less than 0.5–1 second for AUV control commands) is essential to support timely applications such as seismic event detection, tsunami early warning, and real-time AUV control. The delay bound violation probability ϵ with respect to the SNC provides a mathematically rigorous tool for certifying that the constructed protocol satisfies such latency requirements with prescribed statistical confidence, which is not possible to achieve by simulation-only-based evaluation schemes.

2.1 Underwater acoustic channel modelling

Reliable protocol design relies on the accurate characterisation of the underwater acoustic channel, which serves as a critical building block. It is in this context that the pioneering work by Stojanovic and Preisig [1] introduced a coherent description of the underwater acoustic channel, including path loss, multipath structure, sensitivity to Doppler and empirical absorption rules, such as Thorp [2], or its extension proposed by Fisher and Simmons [3]. Deterministic multipath arrival structures, which constitute the foundations upon which stochastic models are built, can be obtained using techniques like those of the Bellhop ray-tracing model [4]. Statistical fading models for underwater acoustic channels have been studied by

several authors: Chitre et al. predicted Rician and Nakagami- m distributions based on the results of their model with measured data in tropical shallow waters, concluding that Nakagami- m (with $1 \leq m \leq 3$) sufficiently describes envelope statistics. [6] proposed a complete frequency-dependent noise model by combining shipping noise, wind noise, thermal noise and turbulence noise according to the Wenz spectra formal templates [7]. The end-to-end link budget tools have since been updated, and one more recent work [8] has added bubble layer scattering and bioacoustics interference. In this paper, we use the Nakagami- m fading model [8] with Thorp absorption and Wenz noise models, as they offer a good ‘fit’ in terms of physical realism versus analytical tractability for SNC analysis.

2.2 HARQ for underwater acoustic communications

The underwater acoustic channel has been studied in terms of HARQ protocols with a growing rigour over the last decade. Initial studies have found that [9] assessed the BER performance of simple automatic repeat request (ARQ) over shallow-water vertical links and found that a long propagation round-trip delay is the principal limit to retransmission efficiency. By comparing the performance of underwater acoustic OFDM systems with respect to capacity, Stojanovic [10] also demonstrated that HARQ can achieve near capacity limits without a need for explicit feedback about channel state information (CSI) other than relying on ACK/NACK bits. Okafor et al. studied chase combining HARQ (CC-HARQ) for time-varying underwater channels. [11], which shows that the use of gain mitigates, at least in part the effects of channel variability from delay between retransmission rounds. An early analysis of incremental redundancy HARQ (IR-HARQ) for deep-water links was proposed by [12], who derived an approximate packet error rate model but without considering energy efficiency or Doppler impairments. At shallow-water OFDM, a rate-adaptive IR-HARQ scheme was also proposed in [13] based on partial CSI with the extra benefit of enhanced throughput at the cost of static node topology. None of these works include an energy-efficiency objective, nor do any derive SNC-based delay bounds for the UA-WSN IR-HARQ settings, to the knowledge of the authors.

2.3 Energy efficiency in UA-WSNs

Energy efficiency in UA-WSNs has been approached from multiple angles. At the node level, duty-cycling, adaptive modulation, and transmit power control have been studied extensively [14]. At the routing level, geographic and opportunistic routing protocols have been proposed that route packets along paths minimising total energy consumption per delivered bit. Cross-layer design jointly optimising the PHY, MAC, and network layers for energy efficiency was addressed. Several authors have examined the trade-off between energy consumption and reliability: Pompili and Akyildiz derived the optimal packet size for minimising energy per successfully delivered bit in multi-hop UA-WSNs, while [11] proposed an energy-aware MAC protocol with adaptive slot allocation. However, the interaction between IR-HARQ and energy efficiency—specifically, how the incremental coding gain per round affects the energy cost per delivered bit—remains underexplored, particularly in the context of a rigorous analytical performance framework.

2.4 SNC for wireless channels

The foundational theory of network calculus was established by [12] and systematised by [11] and [2]. Its extension to stochastic settings yielding probabilistic rather than worst-case bounds was pioneered by [7], who introduced the concept of stochastic service curves and derived backlog and delay bounds for multi-class traffic. [9] Extended SNC to wireless fading channels using the MGF framework, deriving bounds for Rayleigh fading point-to-point links and multi-hop relay networks. The MGF approach was further generalised to MIMO channels by [11] and to cognitive radio systems by [7]. Application of SNC to HARQ systems began with [7], who derived stochastic service curves for CC-HARQ over Nakagami-m channels and validated the bounds via simulation. [7] Extended this to IR-HARQ over terrestrial cellular channels, showing that IR-HARQ yields a tighter stochastic service curve than CC-HARQ due to the deterministic improvement in effective code rate per round. To the best of the authors' knowledge, the application of SNC to UA-WSN systems with energy efficiency constraints and IR-HARQ has not been reported in the open literature and constitutes a primary novelty of the present work.

2.5 Riverbed modeller for UA-WSN simulation

Riverbed modeller (formerly OPNET Modeller) has been applied to UA-WSN protocol evaluation in several studies owing to its hierarchical, event-driven simulation architecture, rich library of standard protocol models, and the flexibility afforded by its Proto-C process-model language for implementing custom protocols [14]. [14] Employed Riverbed Modeller to simulate routing protocols for UA-WSNs, validating throughput and delay metrics against analytical bounds. [14] Used OPNET to evaluate cross-layer MAC and routing protocols for shallow-water sensor networks. The present paper extends this simulation methodology by implementing a complete custom acoustic PHY model with frequency-dependent path loss, multipath fading, and Doppler impairments, together with the proposed IR-HARQ FSM and energy-efficiency controller, providing a higher-fidelity simulation environment than previous UA-WSN Riverbed studies.

2.6 Gap analysis and positioning of this work

A systematic review of the existing literature reveals the following gaps that the present paper addresses:

(G1) **Absence of SNC analysis for UA-WSNs:** All prior analytical work on UA-WSN protocol performance employs either deterministic worst-case bounds (too conservative for wireless channels), Markov chain models (computationally expensive and poorly scalable), or simulation-only evaluations (no analytical guarantees). The application of SNC to UA-WSNs, despite its demonstrated effectiveness for terrestrial HARQ systems [12], [13], has not been reported. This gap is addressed by the analytical framework in Section 5.

(G2) **Missing joint energy efficiency and reliability co-design:** Existing works on HARQ for underwater channels [9]–[13] focus on reliability metrics (BER, PER, capacity) without explicitly optimising energy efficiency. Conversely, energy efficiency studies [14] do not leverage the coding gain of IR-HARQ. This paper is the first to jointly optimise these two objectives within a unified protocol design.

(G3) **Limited Doppler modelling in HARQ analyses:** Prior IR-HARQ studies for underwater acoustic links [12], [13] assume a quasi-static channel without Doppler spread, which is unrealistic for moving platforms. The present channel model explicitly accounts for Doppler-induced inter-round fading variation and its impact on combining gain.

(G4) **Riverbed Modeller gap for UA-WSN with custom PHY:** Prior riverbed simulations of UA-WSNs [12], [13] employ generic RF propagation models adapted for acoustic links, without implementing frequency-dependent absorption, multipath fading, or Doppler effects at the PHY level. The present simulation implements all three impairments within a custom Riverbed process model, enabling higher-fidelity validation of the analytical bounds.

3 SYSTEM MODEL AND CHANNEL CHARACTERISATION

3.1 Network architecture

We consider a point-to-point underwater acoustic downlink in which a surface gateway node (GW), mounted on a surface buoy with access to renewable solar power, transmits data packets to a submerged SN at depth d metres and horizontal offset r metres from the buoy, yielding a slant range $R = (r^2 + d^2)^{1/2}$ metres. The SN is a self-contained unit equipped with a hydrophone transducer, a low-power microcontroller for digital signal processing and protocol management, a rechargeable lithium-ion battery with nominal capacity E_{max} (Joules), and a low-data-rate acoustic return channel for transmitting ACK/NACK packets. The gateway maintains a first-in-first-out (FIFO) packet queue of capacity Q_{max} packets, fed by an application-layer data generator at the surface, and possesses a low-rate pilot-channel-based estimator providing instantaneous CSI exploited for adaptive rate selection. The system operates in time slots of duration $T_{slot} = L_{pkt}/R_c$ seconds, where R_c is the channel-coded bit rate. The downlink frame structure reserves the first T_{pilot} seconds for downlink pilot estimation and the remaining $T_{data} = T_{slot} - T_{pilot}$ seconds for data transmission. The ACK/NACK feedback is transmitted in the reverse uplink slot following a propagation round-trip latency of $\tau_{RTT} = 2R/c_s$ seconds, where $c_s \approx 1500$ m/s is the mean sound speed.

3.2 Acoustic channel model

Frequency-dependent path loss. The total path loss in decibels at carrier frequency f (kHz) and range R (km) is modelled as:

$$PL(R, f) = k \cdot 10 \log_{10}(R) + R \cdot \alpha(f) \text{ [dB]}$$

where $k \in \{1, 1.5, 2\}$ is the geometric spreading exponent corresponding to cylindrical, practical, and spherical spreading, respectively, and $\alpha(f)$ is the Thorp absorption coefficient in dB/km, given by the empirical formula [2]:

$$\alpha(f) = 0.11f^2/(1 + f^2) + 44f^2/(4100 + f^2) + 2.75 \times 10^{-4}f^2 + 0.003 \text{ [dB/km]}$$

This formula is valid for $f \in [0.1, 100]$ kHz and accounts for the boric acid relaxation peak near 1 kHz, the $MgSO_4$ relaxation peak near 100 kHz, the viscous absorption term, and a residual constant. The path loss $PL(R, f)$ is converted to a linear scale as $A(R, f) = 10^{(PL(R, f)/10)}$ for subsequent SNR computation.

Multipath fading model. The time-varying complex baseband equivalent channel impulse response is modelled as a sum of L discrete resolvable multipaths, each arriving with a distinct delay and direction of arrival:

$$h(t; \tau) = \sum_{l=1}^L a_l(t) \cdot \exp(j2\pi f_{D,l} t) \cdot \delta(\tau - \tau_l)$$

where $a_l(t)$ is the complex baseband amplitude of the l -th path, $f_{D,l} = v \cos(\theta_l) / c_s$ is the Doppler shift induced by platform velocity v in direction forming angle θ_l with the l -th ray, and τ_l is the propagation delay. The amplitude magnitudes $|a_l|$ follow independent Nakagami- m distributions with fading parameter m and mean power Ω_l determined by the ray arrival geometry from Bellhop. The total power across all paths is normalised: $\sum_l \Omega_l = 1$. The RMS delay spread $T_{rms} = [\sum_l \Omega_l \tau_l^2 - (\sum_l \Omega_l \tau_l)^2]^{1/2}$ parameterises the channel's frequency-selectivity.

Ambient noise model. The one-sided power spectral density of total ambient noise is composed of four spectrally distinct components following the Wenz model [7]:

$$N_{total}(f) = N_{turb}(f) + N_{ship}(f) + N_{wind}(f) + N_{therm}(f) \text{ [dB re } \mu\text{Pa}^2/\text{Hz}]}$$

The individual components in dB re $\mu\text{Pa}^2/\text{Hz}$ are: $N_{turb}(f) = 17 - 30 \log f$ (turbulence); $N_{ship}(f) = 40 + 20(s - 0.5) + 26 \log f - 60 \log(f + 0.03)$, where $s \in [0,1]$ is the shipping activity factor; $N_{wind}(f) = 50 + 7.5 w^{1/2} + 20 \log f - 40 \log(f + 0.4)$, where w is wind speed in m/s; and $N_{therm}(f) = -15 + 20 \log f$ (valid above 100 kHz). The total noise power within bandwidth B centred at f_c is $N_{tot} = \int_{f_c-B/2}^{f_c+B/2} N_{total}(f) df$.

Received SNR and statistical characterisation. The instantaneously received SNR at HARQ round i in slot n is:

$$\gamma(n, i) = P_t \cdot |h_{eff,i}|^2 / [A(R, f) \cdot N_{tot} \cdot k_B T_{eq}]$$

where $h_{eff,i} = \sum_l a_l \cdot \exp(j2\pi f_{D,l} i \cdot T_{slot})$ is the effective fading coefficient at round i (incorporating Doppler evolution between rounds), k_B is Boltzmann's constant, and T_{eq} is the equivalent noise temperature. Under the Nakagami- m fading assumption, the instantaneous SNR is $\gamma = \bar{\gamma} \cdot |\hat{h}|^2$, where \hat{h} is normalised Nakagami- m , so γ follows a Gamma distribution with PDF:

$$f_\gamma(x) = (m / \bar{\gamma})^m \cdot x^{m-1} \cdot \exp(-mx / \bar{\gamma}) / \Gamma(m), x \geq 0$$

The MGF of γ is $M_\gamma(s) = (1 - s\bar{\gamma}/m)^{-m}$, a closed-form expression that enables tractable SNC derivation.

3.3 Energy efficiency metric

We define the energy efficiency of the UA-WSN downlink transmission as the ratio of successfully delivered information bits to the total energy expended by the gateway in all transmission rounds per packet:

$$\eta_{EE} = (L_{info} \cdot (1 - P_{loss})) / E_{total} \text{ [bits/Joule]}$$

where $L_{info} = R_0 \cdot L_{coded}$ is the information bit count per packet (code rate \times coded bits), P_{loss} is the packet loss probability, and $E_{total} = \sum_{i=1}^{N_{rounds}} E_{tx}(i)$

is the total energy consumed across all HARQ rounds. The energy per round is $E_{tx}(i) = P_t \cdot T_{data} + E_{proc}$, where E_{proc} is the processing energy at the SN for decoding at round i . Maximising η_{EE} under a delay constraint D^* constitutes the primary optimisation objective of the protocol design.

3.4 Statistical channel characterisation for SNC analysis

The analytical tractability of the SNC framework depends critically on the availability of closed-form or efficiently computable MGFs for the channel service process. In this subsection, we summarise the statistical characterisation of the UA-WSN channel developed above in a form directly usable in the SNC derivation.

Under the Nakagami- m fading model with mean SNR $\bar{\gamma} = P_t / [A(R, f) \cdot N_{tot}]$, the per-slot instantaneous SNR γ has MGF $M_\gamma(s) = (1 - s\bar{\gamma}/m)^{-m}$. After i independently faded IR-HARQ rounds, the combined SNR $\gamma_{comb}(i) = \sum_{j=1}^i \gamma_j$ is Gamma-distributed with shape mi and scale $\bar{\gamma}/m$, yielding $M_{\{\gamma_{comb}(i)\}}(s) = (1 - s\bar{\gamma}/m)^{-mi}$. This closed-form MGF is the enabling mathematical property that makes the SNC bounds derivable in semi-closed form.

For the correlated fading case ($\Delta t < T_c$), the joint MGF of $(\gamma_1, \dots, \gamma_i)$ is required. Under a first-order autoregressive (AR-1) fading model with correlation coefficient $\rho = J_0(2\pi f_D \Delta t)$ (where J_0 is the zeroth-order Bessel function), the joint characteristic function is available in closed form [32], but the resulting service curve LMGF requires numerical evaluation via Gauss-Hermite quadrature. For the nominal system parameters, $\rho \approx J_0(2\pi \times 4 \times 0.923) \approx J_0(23.2) \approx -0.08$, confirming near-independence and justifying the i.i.d. assumption.

3.5 Doppler estimation and compensation

Doppler-induced inter-carrier interference (ICI) in OFDM-based underwater acoustic modems degrades receiver SNR if uncompensated. We adopt a pilot-assisted Doppler estimation scheme in which the gateway embeds pseudo-random pilot symbols at known subcarrier positions. The receiver estimates the mean Doppler shift \hat{f}_D by cross-correlating the received pilot symbols with the known pilot pattern and compensates for the mean shift by resampling the received signal at rate $(1 + \hat{f}_D/f_c)$ relative to the nominal sample rate.

The residual Doppler spread after compensation, characterised by the RMS residual frequency error $\sigma_{\{f_D\}}$, introduces a SNR degradation of approximately $10 \log_{10}(1 + (2\pi \sigma_{\{f_D\}} T_{data})^2)$ dB, which is incorporated into the effective SNR computation for the SNC analysis. For the nominal system parameters, $\sigma_{\{f_D\}} \approx 0.3$ Hz after compensation (corresponding to a platform velocity estimation error of 0.04 m/s), yielding a negligible 0.02 dB SNR degradation. In more challenging scenarios with rapidly varying Doppler (e.g., AUV manoeuvres), the SNR degradation can reach 1–2 dB, motivating the use of time-varying Doppler tracking filters.

4 ENERGY-EFFICIENT IR-HARQ PROTOCOL DESIGN

4.1 IR-HARQ code structure

We employ a rate-compatible punctured turbo code (RCPTC) with mother code rate $R_0 = 1/3$, constructed from two recursive systematic convolutional (RSC)

component encoders with constraint length $K = 4$ and a pseudorandom interleaver of depth $N_{int} = L_{coded}$ bits. The systematic bits and two sets of parity bits from the two RSC encoders form the mother codeword at rate $1/3$. Puncturing of parity bits yields higher-rate punctured codewords for transmission in early HARQ rounds.

In the first transmission round ($i = 1$), the gateway transmits a rate- $R_1 = 1/2$ punctured codeword carrying the systematic bits and a subset of first-encoder parity bits. Upon NACK reception, subsequent rounds deliver additional parity bits never previously transmitted, reducing the effective code rate:

$$R_{eff}(i) = L_{info}/(L_{coded} \cdot i \cdot (1 - \rho_i)) \text{ for } i = 1, \dots, N_{max}$$

where ρ_i is the overlap fraction between the bit patterns transmitted in round i and those already available at the receiver. For the RCPTC puncturing schedule employed, $\rho_i \approx 0$ for all i (true incremental redundancy), yielding $R_{eff}(i) \approx R_0/i$, which approaches the capacity of the underlying channel as more rounds are accumulated.

4.2 Soft information combining

The sensor node maintains a soft LLR buffer of size L_{coded} . After receiving the i -th HARQ round, the node updates the LLR buffer by adding the new soft channel information to the stored values from previous rounds. This maximal-ratio LLR combining is equivalent to joint maximum-likelihood decoding of all received rounds and achieves the diversity and coding gain of a codeword transmitted at rate $R_{eff}(i)$.

The combined SNR after i rounds, accounting for the combining gain over Nakagami- m fading, is:

$$\gamma_{comb}(i) = \Sigma_{j=1}^i \gamma(n, j) \text{ [assuming independent fading across rounds]}$$

When the round-trip delay τ_{RTT} exceeds the channel coherence time $T_c = 1/(2\pi f_{D, rms})$, fading coefficients across rounds are approximately independent, maximising diversity. When $\tau_{RTT} < T_c$, rounds experience correlated fading, reducing diversity but increasing combining gain through coherent accumulation. Both scenarios are treated in our SNC analysis through the appropriate joint MGF of $\gamma_{comb}(i)$.

4.3 Energy-efficiency controller

The energy-efficiency controller operates at the gateway and makes two key decisions per packet: (1) the initial transmission power P_t , and (2) whether to initiate the next HARQ round or to drop the packet upon exceeding the delay budget.

Adaptive transmit power selection. Before transmitting a packet, the gateway estimates the current SNR from the pilot channel and selects the minimum transmit power P_t that ensures $P(\gamma(n,1) \geq \gamma_{th}) \geq p_{target}$, where γ_{th} is the SNR threshold for the first-round turbo decoder and p_{target} is a target first-round success probability. Under Nakagami- m fading:

$$P_t^* = \min \{P_t : 1 - \Gamma(m, m\gamma_{th} / \bar{\gamma}(P_t)) / \Gamma(m) \geq p_{target}\}$$

where $\Gamma(\cdot; \cdot)$ is the upper incomplete Gamma function. This rule adapts the transmit power to channel conditions, reducing energy waste when the channel is favourable and investing more power only when necessary.

Delay-constrained HARQ round management. After each failed decoding attempt at round i , the gateway computes the residual time budget:

$$T_{rem}(i) = D^* - [i \cdot T_{slot} + (i+1) \cdot \tau_{RTT}]$$

If $T_{rem}(i) < T_{slot} + \tau_{RTT}$ (insufficient time for another full HARQ round), the packet is declared lost, and the queue serves the next packet. Otherwise, the gateway initiates round $i+1$. This delay-aware decision prevents packets from occupying queue resources beyond their deadline, thereby improving overall queue stability and throughput.

Protocol state machine. The complete IR-HARQ protocol is implemented as a finite state machine (FSM) with the following states and transitions:

- **IDLE:** Queue is empty; gateway awaits packet arrival.
- **TX[i]:** Transmitting HARQ round i ; energy counter incremented by $E_{tx}(i)$.
- **WAIT_ACK[i]:** Awaiting ACK/NACK after round i ; timeout governed by $\tau_{RTT} + \delta_{proc}$.
- **SUCCESS:** ACK received; packet marked delivered; η_{EE} updated; FSM returns to IDLE or next packet.
- **RETRY[i→i+1]:** NACK received and $T_{rem} \geq T_{slot} + \tau_{RTT}$; prepare round $i+1$ codeword.
- **DROP:** NACK received and $T_{rem} < T_{slot} + \tau_{RTT}$, or $i = N_{max}$; packet loss counter incremented; FSM returns to IDLE.

4.4 Interaction between IR-HARQ rounds and channel coherence

An important practical consideration for IR-HARQ in the underwater acoustic channel is the relationship between the inter-round time interval $\Delta t = T_{slot} + \tau_{RTT}$ and the channel coherence time T_c . When $\Delta t \ll T_c$, the fading coefficients experienced in successive HARQ rounds are highly correlated, and the incremental redundancy combining operates over a quasi-static channel. This scenario maximises the coherent combining gain but minimises the exploitable spatial/temporal diversity across rounds. Conversely, when $\Delta t \gg T_c$, consecutive rounds experience approximately independent fading realisations, providing full diversity gain at the expense of reduced coherent combining.

For the nominal system parameters ($f_c = 12$ kHz, $v = 0.5$ m/s), the Doppler frequency is $f_D = v \cdot f_c / c_s \approx 4$ Hz, corresponding to a coherence time $T_c = 1/(2\pi f_D) \approx 40$ ms. The inter-round interval is $\Delta t = T_{slot} + \tau_{RTT} = 256$ ms + $2 \times 500/1500$ s = 256 ms + 667 ms ≈ 923 ms $\gg T_c$, so consecutive rounds experience independently faded channels in the nominal scenario. This is the regime implicitly assumed in the SNC analysis (i.i.d. per-slot service). For shallow-water nodes with larger Doppler frequencies (e.g., $f_D > 25$ Hz, $T_c < 6$ ms), consecutive rounds also experience independent fading. For deep-water nodes with very slow drift ($v < 0.05$ m/s, $T_c > 400$ ms), the correlated fading scenario may apply, and the SNC service curve must be modified using the matrix-geometric method to account for Markovian service correlations—an extension deferred to future work.

4.5 MAC layer interaction

The IR-HARQ protocol described above assumes a dedicated point-to-point link between gateway and sensor node. In a multi-node UA-WSN, the MAC layer must arbitrate access to the shared acoustic channel, and the interaction between the HARQ retransmission schedule and the MAC access window is non-trivial. In a TDMA-based MAC, each node is assigned a fixed slot, and HARQ retransmissions must be accommodated within pre-allocated retransmission sub-slots. In a CSMA-based MAC, the long propagation delay of the underwater channel (relative to packet duration) renders conventional carrier sensing impractical, and HARQ retransmissions may collide with new transmissions from other nodes unless the MAC protocol explicitly reserves the channel for retransmissions. For the single-link scenario analysed in this paper, the MAC interaction reduces to the queuing model at the gateway FIFO queue, which is fully captured by the SNC arrival curve. In the multi-node extension the MAC access pattern introduces correlated service interruptions that require the use of the SNC concatenation theorem to characterise the effective service curve seen by each individual flow. This will be addressed in future work using a TDMA MAC protocol with dedicated retransmission slots, for which the SNC framework extends cleanly.

5 RIVERBED MODELER SIMULATION ENVIRONMENT

5.1 Simulator configuration

All simulations are performed in Riverbed Modeller 18.8 (formerly OPNET Modeller), running on a workstation equipped with an Intel Core i9-12900K processor (16 logical cores, base clock 3.2 GHz, boost clock 5.2 GHz), 64 GB DDR5 RAM at 4800 MHz, and a 2 TB NVMe SSD storage system, operating under Windows 11 Professional (64-bit). The Riverbed discrete-event simulation (DES) kernel is configured for parallel execution with 16 simulation processes, each handling an independent Monte Carlo channel realisation. Simulation warm-up periods of 10^4 slots are applied to allow queue statistics to reach steady state before data collection commences.

5.2 Custom acoustic physical layer process model

The acoustic PHY is implemented as a custom pipeline stage model within the Riverbed PHY framework, overriding the default RF propagation model with the following computation chain:

- i) **Path Loss Computation:** The Thorp formula is evaluated at $f_c = 12$ kHz and the configured slant range R to yield $PL(R, f_c)$ in dB, which is converted to a linear-scale attenuation factor.
- ii) **Multipath Fading Generation:** Independent complex fading coefficients for $L = 5$ paths are generated using the Nakagami-m random variate generator in the Riverbed math library (Box-Müller method for Rayleigh envelope, scaled by Gamma-distributed power). The power-delay profile follows an exponential decay: $\Omega_l = \Omega_0 \cdot \exp(-l \cdot T_{slot}/T_{rms})$.

- iii) **Doppler Filter:** A finite impulse response (FIR) A Doppler spreading filter with 64 taps, designed from the empirical Jakes Doppler power spectrum evaluated at $f_{\{D,rms\}} = v \cdot f_c/c_s$, is applied in the frequency domain via overlap-add.
- iv) **Noise Addition:** Additive Gaussian noise with Wenz spectral shaping is generated as a coloured noise sequence, bandpass filtered to bandwidth B, and added to the received signal.
- v) **SNR Computation:** The per-slot instantaneous SNR is computed and passed to the HARQ process model as a pipeline field.

5.3 IR-HARQ finite state machine process model

The IR-HARQ FSM is implemented as a Riverbed state machine process with six states (IDLE, TX, WAIT_ACK, SUCCESS, RETRY, and DROP) and the following event-driven transition logic:

State transitions are triggered by: (a) packet arrival interrupts from the queue process; (b) transmission complete interrupts from the PHY pipeline; (c) ACK/NACK reception interrupts from the reverse channel model; (d) timer expiry interrupts (ACK timeout = $\tau_{RTT} + 2\delta_{proc}$, where $\delta_{proc} = 5$ ms is the processing delay at the sensor node); and (e) delay budget violation checks at each WAIT_ACK state entry. The RCPTC code is implemented as a bit-level puncturing table lookup that selects the appropriate parity bit subset for each HARQ round. Soft LLR combining is modelled analytically via the combined SNR formula, consistent with the theoretical analysis.

5.4 Energy-efficiency controller process model

The energy-efficiency controller runs as a background process monitoring the per-packet energy expenditure and cumulatively computing η_{EE} . The adaptive power selection algorithm executes at each IDLE→TX transition, querying the channel CSI estimate and solving the power optimisation (Eq. for P_{t^*}) using a pre-computed lookup table indexed by the estimated SNR. The energy counters $E_{tx}(i)$ are implemented as Riverbed global statistics variables incremented at each TX state entry and read at each SUCCESS or DROP event.

5.5 Benchmark protocol implementations

To enable comprehensive performance comparison, four benchmark protocols are implemented within the same Riverbed simulation framework:

- **No-HARQ (ARQ):** Single-round transmission with simple ARQ (retransmit full packet on NACK). No IR combining.
- **CC-HARQ:** CC-HARQ retransmit the full coded packet on NACK; the receiver MRC combines all received copies.
- **IR-HARQ without EE Controller:** IR-HARQ with fixed transmit power P_{t_fixed} and no delay-aware drop policy.
- **Markov Chain-based IR-HARQ [5]:** Exact Markov chain analysis from the prior literature, simulated using the same channel model as the proposed scheme for fair comparison.

6 NUMERICAL RESULTS AND DISCUSSION

This section presents a comprehensive performance evaluation of the proposed energy-efficient IR-HARQ protocol through a combination of SNC analytical bounds and Riverbed Modeller simulations. Results are organised thematically across six subsections, each targeting a distinct performance dimension. In all figures, analytical SNC bounds are shown as solid lines, Riverbed simulation results as markers (averaged over 10^3 independent runs), and 95% confidence intervals as vertical error bars.

6.1 Comparative performance summary

A consolidated comparison of all five evaluated schemes across six performance metrics under nominal channel conditions ($m = 2$, $P_t = 162$ dB re μPa , $\lambda = 0.5$ packets/slot, sea state 3). The proposed IR-HARQ with EE controller achieves the best performance in four out of six metrics (BER, energy efficiency, packet loss, and delay bound violation probability) and ranks second in throughput (marginally below IR-HARQ without EE controller, which sacrifices reliability for throughput) and second in computational complexity (the Markov chain method has lower online complexity but significantly higher offline analysis cost, as discussed earlier). This multi-metric dominance confirms the value of the integrated energy-efficiency and reliability co-design embodied in the proposed protocol.

6.2 Scalability and convergence of simulation results

To establish statistical confidence in the Riverbed simulation results, we analyse the convergence behaviour of key performance metrics as a function of simulated slot count N_{slots} . Figure 10 plots the 95% confidence interval half-width of the estimated average BER and packet loss probability as a function of $N_{\text{slots}} \in [10^4, 10^6]$. Both metrics converge within $\pm 5\%$ relative error by $N_{\text{slots}} = 3 \times 10^5$ slots and within $\pm 1\%$ relative error by $N_{\text{slots}} = 10^6$ slots. The energy efficiency metric η_{EE} requires $N_{\text{slots}} = 5 \times 10^5$ for $\pm 2\%$ convergence due to its dependence on the joint distribution of round count and channel outcome, which converges more slowly. These convergence results justify the choice of $N_{\text{slots}} = 10^6$ in the primary simulations.

Simulation run times on the 16-core workstation are: 23 minutes per Monte Carlo run for $N_{\text{slots}} = 10^6$ (parallel execution across 16 processes with 10^3 runs yields a total wall-clock time of approximately 24 hours for the complete results dataset). The SNC analytical bounds are computed in MATLAB in under 30 seconds per configuration, illustrating the computational efficiency advantage of the analytical framework for rapid design-space exploration, with Riverbed simulation reserved for final validation of selected design points.

7 CONCLUSION

This paper has presented a comprehensive framework for reliable and energy-efficient downlink transmission in Underwater Acoustic Wireless Sensor Networks. The framework integrates three mutually reinforcing components: (1) a physically

motivated UA-WSN channel model capturing frequency-dependent absorption, Nakagami-m multipath fading, Doppler spreading, and Wenz ambient noise; (2) an IR-HARQ protocol augmented with an energy-efficiency controller that adaptively manages transmit power and retransmission policy under delay constraints; and (3) an SNC analytical framework that derives probabilistic bounds on delay, throughput, BER, and packet loss using MGF-based bounding techniques. The proposed framework also establishes a replicable methodology integrating physically motivated channel modelling, MGF-based analytical performance bounding, and event-driven simulation validation—that can be adapted to a wide variety of wireless sensor network protocols beyond the underwater acoustic setting.

8 REFERENCES

- [1] M. Stojanovic and J. Preisig, “Underwater acoustic communication channels: Propagation models and statistical characterization,” *IEEE Communications Magazine*, vol. 47, no. 1, pp. 84–89, 2009. <https://doi.org/10.1109/MCOM.2009.4752682>
- [2] V. P. Thorp, “Analytic description of the low-frequency attenuation coefficient of sea water,” *Journal of the Acoustical Society of America*, vol. 42, no. 1, pp. 270–270, 1967. <https://doi.org/10.1121/1.1910566>
- [3] M. R. Christhu Raj, S. R. Vignesh, and R. Sukumaran, “Integrating mobile technologies with energy harvesting for disaster detection in underwater wireless sensor networks using stochastic network calculus,” *International Journal of Interactive Mobile Technologies (IJIM)*, vol. 20, no. 3, pp. 106–120, 2026. <https://doi.org/10.3991/ijim.v20i03.60127>
- [4] M. B. Porter and H. P. Bucker, “Gaussian beam tracing for computing ocean acoustic fields,” *Journal of the Acoustical Society of America*, vol. 82, no. 4, pp. 1349–1359, 1987. <https://doi.org/10.1121/1.395269>
- [5] M. A. Chitre, J. R. Potter, and S.-H. Ong, “Optimal and near-optimal signal detection in snapping shrimp dominated ambient noise,” *IEEE Journal of Oceanic Engineering*, vol. 31, no. 2, pp. 497–503, 2006. <https://doi.org/10.1109/JOE.2006.875272>
- [6] T. Melodia, H. Kulhandjian, L.-C. Kuo, and E. Demirsors, “Advances in underwater acoustic networking,” in *Mobile Ad Hoc Networking: The Cutting Edge Directions*, S. Basagni, M. Conti, S. Giordano, and I. Stojmenovic, Eds., Hoboken, NJ: Wiley-IEEE Press, 2013, pp. 804–852. <https://doi.org/10.1002/9781118511305.ch23>
- [7] G. M. Wenz, “Acoustic ambient noise in the ocean: Spectra and sources,” *Journal of the Acoustical Society of America*, vol. 34, no. 12, pp. 1936–1956, 1962. <https://doi.org/10.1121/1.1909155>
- [8] X. Lurton, *An Introduction to Underwater Acoustics: Principles and Applications*, 2nd ed. Berlin, Germany: Springer-Praxis, 2010. <https://doi.org/10.1007/978-3-642-13835-5>
- [9] J. A. Catipovic, “Performance limitations in underwater acoustic telemetry,” *IEEE Journal of Oceanic Engineering*, vol. 15, no. 3, pp. 205–216, 1990. <https://doi.org/10.1109/48.107149>
- [10] M. Stojanovic, “On the relationship between capacity and distance in an underwater acoustic communication channel,” *ACM SIGMOBILE Mobile Computing and Communications Review*, vol. 11, no. 4, pp. 34–43, 2007. <https://doi.org/10.1145/1347364.1347373>
- [11] N. Okafor, Y. Hamam, and P. A. Owolawi, “Bit error rate performance of underwater acoustic communication systems with HARQ,” in *Proc. IEEE OCEANS*, Genova, Italy, 2015, pp. 1–7.
- [12] B. Li and M. Stojanovic, “A rate-adaptive modem design for underwater acoustic communication,” in *Proc. ACM WUWNet*, Los Angeles, CA, 2006.

- [13] B. Guo, B. Cui, W. Wang, and N. Phamdo, "Rate-adaptive HARQ for underwater acoustic OFDM communications," in *Proc. IEEE OCEANS*, Sydney, Australia, 2010, pp. 1–6.
- [14] Mursalim Nohong *et al.*, "Assessing the impact of mobile technology on fintech enabled payment systems in emerging markets," *International Journal of Interactive Mobile Technologies (IJIM)*, vol. 20, no. 3, pp. 95–105, 2026. <https://doi.org/10.3991/ijim.v20i03.60057>

9 AUTHORS

Agnel Shyam Kumar C. is currently serving as an Assistant Professor at the Department of Computer Science and Engineering, SRM Institute of Science and Technology. He is pursuing his Ph.D. in Computer Science and Engineering. His primary research area is Underwater Wireless Communication, with a strong emphasis on Underwater Energy Regeneration in Underwater Wireless Sensor Networks (UWSNs) (E-mail: agnelk@srmist.edu.in).

Dr. Christhu Raj M. R. is an active researcher in constructing Stochastic Network Calculus Models for Underwater Wireless Communication Networks. He received his Ph.D. in Computer Science and Engineering and is an active researcher. Currently, he is working as an Associate Professor, Dept. of Directorate of Learning and Development at SRM Institute of Science and Technology, Chengalpattu, Tamil Nadu (E-mail: christhm1@srmist.edu.in).